

A System Identification-based Modeling Framework of Bidirectional DC-DC Converters for Power Grids

Gabriel E. Mejia-Ruiz, Mario R. A. Paternina, Juan R. Rodriguez R., Juan M. Ramirez, Alejandro Zamora-Mendez, and Guillermo Bolivar-O.

Abstract—This paper proposes a system identification framework based on eigensystem realization to accurately model power electronic converters. The proposed framework affords an energy-based optimal reduction method to precisely identify the dynamics of power electronic converters from simulated or actual raw data measured at the converter's ports. This method does not require any prior knowledge of the topology or internal parameters of the converter to derive the system modal information. The accuracy and feasibility of the proposed method are exhaustively evaluated via simulations and practical tests on a software-simulated and hardware-implemented dual active bridge (DAB) converter under steady-state and transient conditions. After various comparisons with the Fourier series-based generalized average model, switching model, and experimental measurements, the proposed method attains a root mean square error (RMSE) of less than 1% with respect to the actual raw data. Moreover, the computational effort is reduced to 1/8.6 of the Fourier series-based model.

Index Terms—Dual active bridge, eigensystem realization algorithm, generalized average model, power electronic converter, identification.

I. INTRODUCTION

OVER the years, power systems with multiple power electronic converters have considerably evolved [1]–[3]. The modern power systems are characterized by an ex-

ceptional combination of power electronic converters enabling the interface with renewable energy resources, energy storage resources, microgrids, and DC loads, as depicted in Fig. 1. These controllable converters are capable of incorporating intelligence into the power system because they are equipped with communication capabilities and can make autonomous control decisions at the installation site. However, the interaction between power electronic converters and power systems creates complex dynamic behaviors in the entire grid [1]. Moreover, system-level designers and power system operators require robust tools to model and analyze the network and its elements. In particular, power electronic converters are spread over active distribution networks consisting of commercial off-the-shelf converters, which need to be modelled. Typically, manufacturers do not provide the behavioral model of converters; and consequently, the theoretical and simulation analyses for interconnection and control purposes are rendered infeasible. In power systems with a variety of converter brands, this problem can be more complex.

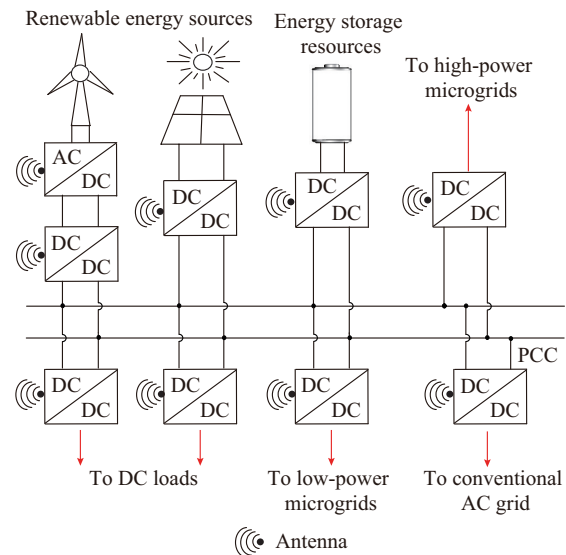


Fig. 1. DC grid scheme.

Although most of these converters can control the power flow among the elements, the high penetration of these devices can increase the probability of conflict between their

Manuscript received: December 1, 2020; revised: February 10, 2021; accepted: April 8, 2021. Date of CrossCheck: April 8, 2021. Date of online publication: April 21, 2021.

This work was supported by the Project Support Program for Research and Technological Innovation of UNAM (DGAPA, PAPIIT-2021) (No. TA101421) and the strategic project PE-A-04 of CEMIE-Redes.

This article is distributed under the terms of the Creative Commons Attribution 4.0 International License (<http://creativecommons.org/licenses/by/4.0/>).

G. E. Mejia-Ruiz, M. R. A. Paternina (corresponding author), and J.R. Rodriguez R. are with the Department of Electrical Engineering, National Autonomous University of Mexico (UNAM), Mexico City, Mexico (e-mail: gabriel.mejia.ruiz@comunidad.unam.mx; mra.paternina@fib.unam.mx; jrrodriguez@fi-b.unam.mx).

J. M. Ramirez is with the Department of Electrical Engineering, Center for Research and Advanced Studies (CINVESTAV), Guadalajara, Mexico (e-mail: jramirez@gdl.cinvestav.mx).

A. Zamora-Mendez is with the Electrical Engineering Faculty, Michoacan University of Saint Nicholas of Hidalgo (UMSNH), Morelia, Mexico (e-mail: azamoram@umich.mx).

G. Bolivar-O. is with the Engineering Faculty, Corporacion Universitaria Minuto de Dios-UNIMINUTO, Bello, Colombia (e-mail: guillermo.bolivar@uniminuto.edu).

DOI: 10.35833/MPCE.2020.000836

control actions and conventional control devices installed in power systems. Thus, it is necessary to develop sophisticated control systems capable of coordinating the entire operation. In this context, the power electronic converter model is essential for analyzing, designing, and controlling active networks with high integration of power electronic converter [1], [2].

In contrast, simulations including those of power electronic converters are constrained by the contradiction between the short simulation time step for describing the transient behaviors and the sizable computational loads. These constraints lead to two different approaches for representing the switching power electronic converter: ① theoretical derivation or phenomenological approach; and ② measurement-based approach [3]. The former has traditionally relied on the detailed knowledge of internal parameters and physical laws that relate the converter variables by managing a considerable number of parameters and a complex set of equations. All of these require high computational resources for simulation. By contrast, the measurement-based approach only requires the input and output signals of the converter and their sampling rates. It solely relies on the behavior observed at the terminals of the equipment [3]-[6].

For large-scale systems, the simulation models should be formulated as simple as possible; nevertheless, they should retain relevant information. To reduce the computational burden and gain additional system-level details, the use of identification techniques such as the so-called black-box behavioral model, has been widely reported [7]-[9]. These methods are capable of analyzing the time-domain system re-

sponse in a simulator with low computational requirements [10], [11].

In previous decades, various modeling techniques using phenomenological approaches have been widely introduced [1], [2], [12]. Among these, the generalized averaging process, which is capable of representing any arbitrary periodic waveforms through a Fourier series (FS) approach, is widely employed for the converters that include AC dynamic variables. However, all of these phenomenological modeling methods require detailed and precise knowledge of the internal converter parameters and time-consuming simulations [5], [13], [14]. Although black-box identification techniques have been widely employed in engineering applications [8], [9], their applications in power electronic converters have only been reported in a few publications [11], [15]-[17].

A practical computer-aided identification method for power electronic converters has been presented in [15]. The technique requires prior knowledge of the performance characteristics of other similar converters. The use of commercial software is necessary to obtain the interconnection data for all elements inside the converter. In [11], the ability of the proposed generic frequency-domain model to predict the voltage and current in the converter is demonstrated. This representation is only valid for the converters with pulse-width modulation. In [16], a converter identification model employing a linear state estimator is introduced; however, this system has only been tested for fault identification.

The comparison of the various types of models for power electronic converters are summarized in Table I.

TABLE I
COMPARISON OF VARIOUS TYPES OF MODELS FOR POWER ELECTRONIC CONVERTERS

Model	Accuracy for predicting steady-state behavior	Accuracy for open-loop dynamic response	Whether model represents transformer AC current	Model order	Means of model validation	Computational requirements	Applicability
Switching model [18], [19]	Very high	Very high	Yes	2 nd order	Simulations and experimental tests	Very high	Design of nonlinear controller, study of highly nonlinear phenomena, and stability analysis
Generalized average model by FS [4], [13], [20]-[22]	High	High	Yes	3 rd order	Simulations and experimental tests	High	Simulation and design at circuit level, design of circuit controller
Steady-state model [23]-[25]	High	None	Yes	Not applicable	Simulations and experimental tests	Medium	Determination of operative modes, design of converter parameters
Discrete-time model [26]-[28]	High	High	No	2 nd order	Experimental tests with high error	High	Design of digital controller
State-space model [29], [30]	Medium	Low	No	5 th and 7 th order	Experimental tests	Medium	Simulation of DC variables at circuit level
Proposed ERA black-box model	Very high	Very high	Yes	4 th and 12 th order	Simulations and experimental tests	Low	Simulation and design at system level

Most of the proposed models are focused on the design of parameters as well as converter controllers and operating modes, neglecting the computational efficiency requirements for the simulation in large-scale systems. In contrast, the eigensystem realization algorithm (ERA) has been widely used for several decades to model power systems, demonstrating a performance level suitable for multi-signal modeling [31]-

[33]. However, its use in electronic converters has never been explored. Accordingly, this paper extends the applicability of the ERA approach to precisely identify the dynamic behavior of power converters using the measurements obtained from these devices. The primary contributions of the proposed method are identified below.

This paper introduces a novel implementation of the ERA

to accurately define the modal information of converter systems, extending its applicability from low-frequency to high-frequency dynamics. This proposed method resolves the high-frequency (HF) problems reported in [32] - [34] and overcomes the absence of information resulting from the neglect of converter manufacturers. The approach does not require any prior knowledge of the structure or internal parameters associated with commercial off-the-shelf converters.

The ERA approach exploits the higher singular values that correspond to the highest energy of the physical system. This represents an energy-based optimal reduction model for the identified converter, thus providing a simplified converter model that reduces the computational effort and simulation time.

The effectiveness of the proposed identification technique is assessed by comparing the modeling approaches extensively reported in the technical literature. With a root-mean-square error (RMSE) of less than 1%, the derived results demonstrate that the proposed method can accurately represent the dynamic behavior of the power converter. Moreover, the computational effort is reduced to 1/8.6 of the FS-based generalized average model.

Typical of the dynamic characteristics of multivariate systems, the replication of the detailed modeling process proposed in this paper may be applied to other power converters.

This paper also derives the FS-based generalized due active bridge (DAB) model in detail with a novel set of state variables, including the power losses of the coupling transformer. The computational efficiency of this model is exhaustively compared with that of the ERA model.

The remainder of this paper is structured as follows. The DAB topology and converter modeling through the ERA are introduced in Section II. The derivation of the switching and FS-based generalized average models is presented in Section III for comparison. The experimental tests and simulation results validating the proposed approach are explicated in Section IV. Finally, the concluding remarks are summarized in Section V.

II. DAB TOPOLOGY AND CONVERTER MODELING THROUGH ERA

A. Circuit Topology

The DAB converter features bidirectional power flow, inherent soft switching, high power density, galvanic isolation, buck-boost functionality, and high-efficiency voltage conversion [5], [13], [14]; its topology is depicted in Fig. 2. This converter is composed of two single-phase active bridges (one on the primary (input) side, and the other on the secondary (output) side), an HF transformer, a capacitor C on the output side with eight switches Q_1 - Q_8 , and a resistive load R on the output side. The HF transformer galvanically isolates the system's input and output, and provides energy storage through the winding leakage inductance L_l . The losses in the transformer are concentrated in the series resistance R_t . N is the turn ratio of the HF transformer. The input voltage and current are represented in the circuit by v_i and i_i , re-

spectively. The voltage and current on the primary side of the transformer are v_p and i_p , respectively. The voltage and current on the secondary side of the transformer are v_s and i_2 , respectively. The output voltage and current are v_o and i_R , respectively. i_s is the addition of the current of C and i_R .

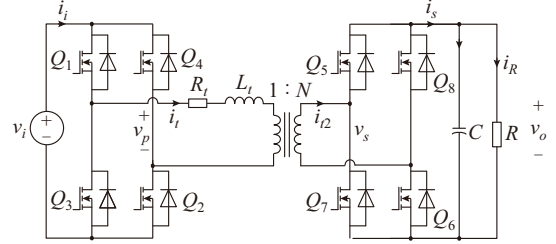


Fig. 2. DAB topology.

B. DAB Converter Modeling Through Eigensystem Realization

The resolution of DAB converter modeling as a discrete-time system identification problem is presented in this subsection [35], where the Markov parameters A , B , C , and D are unknown. In this case, the discrete-time system representation is given by:

$$\begin{cases} \mathbf{x}(k+1) = \mathbf{A}\mathbf{x}(k) + \mathbf{B}\mathbf{u}(k) \\ \mathbf{y}(k) = \mathbf{C}\mathbf{x}(k) + \mathbf{D}\mathbf{u}(k) \end{cases} \quad (1)$$

where A , B , C , and D are the time invariant matrices; and $\mathbf{u}(k)$, $\mathbf{x}(k)$, and $\mathbf{y}(k)$ are the input vector, state vector, and output measurement vector for the k^{th} discrete time instant, respectively.

Given an output measurement vector $\mathbf{y}(k) \in \mathbf{R}^{N \times 1}$, the identification problem consists of determining the Markov parameters for unit impulse input, such that \mathbf{y} is a result yielded by the state-variable equations. If a sequence of noiseless measurements of the input-output pairs of a discrete time system is assumed, the consideration and generation of a zero-state response to the known input sequence, $\mathbf{u}(0), \mathbf{u}(1), \dots, \mathbf{u}(N)$, are enabled. The output sequence is presented as [35]:

$$\begin{cases} \mathbf{y}(0) = \mathbf{D}\mathbf{u}(0) \\ \mathbf{y}(1) = \mathbf{C}\mathbf{B}\mathbf{u}(0) + \mathbf{D}\mathbf{u}(1) \\ \mathbf{y}(2) = \mathbf{C}\mathbf{A}\mathbf{B}\mathbf{u}(0) + \mathbf{C}\mathbf{B}\mathbf{u}(1) + \mathbf{D}\mathbf{u}(2) \\ \vdots \\ \mathbf{y}(N-1) = \mathbf{C}\mathbf{A}^{N-1}\mathbf{B}\mathbf{u}(0) + \mathbf{C}\mathbf{A}\mathbf{B}\mathbf{u}(1) + \dots + \mathbf{D}\mathbf{u}(N-1) \end{cases} \quad (2)$$

The input and output sequences of the ERA-based model can be obtained using either the experimental measurements from the converter or simulated data from the phenomenological model if the topology and converter parameters are available. Hence, the simulation at the system level that involves multiple converters interacting in an electrical network can benefit from the computational efficiency of the ERA model.

In matrix form, the output sequence becomes that given in (3), where the relationship between the input and output data, which is dependent on the Markov parameters, is established as:

$$\begin{bmatrix} \mathbf{y}(0) \\ \mathbf{y}(1) \\ \mathbf{y}(2) \\ \vdots \\ \mathbf{y}(N-1) \end{bmatrix} = \begin{bmatrix} \mathbf{D} & \mathbf{0} & \mathbf{0} & \dots & \mathbf{0} \\ \mathbf{CB} & \mathbf{D} & \mathbf{0} & \dots & \mathbf{0} \\ \mathbf{CAB} & \mathbf{CB} & \mathbf{D} & \dots & \mathbf{0} \\ \vdots & \vdots & \vdots & \ddots & \vdots \\ \mathbf{CA}^{N-1}\mathbf{B} & \mathbf{CAB} & \mathbf{CB} & \dots & \mathbf{D} \end{bmatrix} \begin{bmatrix} \mathbf{u}(0) \\ \mathbf{u}(1) \\ \mathbf{u}(2) \\ \vdots \\ \mathbf{u}(N-1) \end{bmatrix} \quad (3)$$

The impulse response is assumed for the system in (1) and $k > 0$; hence, the interdependency state $\mathbf{x}(k)$ and output $\mathbf{y}(k)$ in terms of the Markov parameters yield:

$$\begin{cases} \mathbf{x}(k) = \mathbf{A}^{k-1}\mathbf{B} \\ \mathbf{y}(k) = \mathbf{CA}^{k-1}\mathbf{B} \end{cases} \quad (4)$$

Moreover, the block Hankel matrix $\mathbf{H}(k)$ for the n^{th} output is defined as:

$$\mathbf{H}(k) = \begin{bmatrix} \mathbf{CA}^{k-1}\mathbf{B} & \mathbf{CA}^k\mathbf{B} & \dots & \mathbf{CA}^{k-1+n}\mathbf{B} \\ \mathbf{CA}^k\mathbf{B} & \mathbf{CA}^{k+1}\mathbf{B} & \dots & \mathbf{CA}^{k+n}\mathbf{B} \\ \vdots & \vdots & \ddots & \vdots \\ \mathbf{CA}^{k-1+n}\mathbf{B} & \mathbf{CA}^{k+n}\mathbf{B} & \dots & \mathbf{CA}^{k-1+2n}\mathbf{B} \end{bmatrix} \quad (5)$$

This can be also represented by (6):

$$\mathbf{H}(k) = \begin{bmatrix} \mathbf{C} \\ \mathbf{CA} \\ \vdots \\ \mathbf{CA}^n \end{bmatrix} \mathbf{A}^{k-1} [\mathbf{B} \quad \mathbf{AB} \quad \dots \quad \mathbf{A}^n\mathbf{B}] \quad (6)$$

Then, (6) can be generalized as:

$$\mathbf{H}(k) = \xi \mathbf{A}^{k-1} \mathbf{B} \quad (7)$$

where ξ and $\mathbf{A}^{k-1}\mathbf{B}$ are the observability and controllability matrices, respectively. It can redefine the Hankel matrix (5) relative to the function of the Markov parameters $\mathbf{y}(k)$ ($k = 0, 1, \dots, 2N$). Thus, $\mathbf{H}(k)$ and $\mathbf{H}(k+1)$ can be described as:

$$\mathbf{H}(k) = \begin{bmatrix} \mathbf{y}(k) & \mathbf{y}(k+1) & \dots & \mathbf{y}(k+N) \\ \mathbf{y}(k+1) & \mathbf{y}(k+2) & \dots & \mathbf{y}(k+N+1) \\ \vdots & \vdots & \ddots & \vdots \\ \mathbf{y}(k+N) & \mathbf{y}(k+N+1) & \dots & \mathbf{y}(k+2N) \end{bmatrix} \quad (8)$$

$$\mathbf{H}(k+1) = \begin{bmatrix} \mathbf{y}(k+1) & \mathbf{y}(k+2) & \dots & \mathbf{y}(k+N+1) \\ \mathbf{y}(k+2) & \mathbf{y}(k+3) & \dots & \mathbf{y}(k+N+2) \\ \vdots & \vdots & \ddots & \vdots \\ \mathbf{y}(k+N+1) & \mathbf{y}(k+N+2) & \dots & \mathbf{y}(k+2N+1) \end{bmatrix} \quad (9)$$

By substituting $k=1$ and $k=2$ in (7), the Hankel matrices are given by:

$$\begin{cases} \mathbf{H}(1) = \xi \mathbf{B} \\ \mathbf{H}(2) = \xi \mathbf{AB} \end{cases} \quad (10)$$

The rank of Hankel matrix \mathbf{H} is considerably higher than the system order due to measurement noise. A reduced-order model can be derived using its singular values ordered from the highest to the lowest. To proceed with such calculation, the singular value decomposition is applied to $\mathbf{H}(1)$, resulting in $\mathbf{H}(1) = \mathbf{PSQ}^T$, where \mathbf{P} and \mathbf{Q} are the left and right singular vectors, respectively, and \mathbf{S} is a diagonal matrix of singular eigenvalues (non-negative). Thus, the approximation order becomes the number of nonzero singular values. Then, $\mathbf{H}(1)$ can be partitioned into $\mathbf{H}(1) = \mathbf{PS}^{1/2}\mathbf{S}^{1/2}\mathbf{Q}^T$ with $\xi = \mathbf{PS}^{1/2}$ and $\mathbf{B} = \mathbf{S}^{1/2}\mathbf{Q}^T$ in (10). Hence, the discrete-time system matrices

in (1) are derived from (10) as:

$$\begin{cases} \mathbf{A} = \mathbf{S}^{-1/2} \mathbf{P}^T \mathbf{H}(2) \mathbf{QS}^{-1/2} \\ \mathbf{B} = \mathbf{S}^{1/2} \mathbf{Q}^T \\ \mathbf{C} = \mathbf{PS}^{1/2} \\ \mathbf{D} = \mathbf{y}(0) \end{cases} \quad (11)$$

After estimating the Markov parameters in (1) in discrete time, the continuous-time state-space model is derived using the MATLAB function *d2c*. The system is then transformed into a state-space representation in continuous time using the MATLAB function *ss*. Finally, the transfer function becomes:

$$\mathbf{H}(s) = \mathbf{C}(s\mathbf{I} - \mathbf{A})^{-1}\mathbf{B} + \mathbf{D} \quad (12)$$

C. ERA Analysis with Multiple Outputs

For numerous output channels, the matrix $\mathbf{Y}_m \in \mathbf{R}^{N \times m}$ is shaped by m column arrays corresponding to single channels as:

$$\mathbf{Y}_m = [\mathbf{y}^{(1)} \quad \mathbf{y}^{(2)} \quad \dots \quad \mathbf{y}^{(q)} \quad \dots \quad \mathbf{y}^{(m)}] \quad (13)$$

where the q^{th} column is represented by $\mathbf{y}^{(q)} = [\mathbf{y}(0), \mathbf{y}(1), \dots, \mathbf{y}(N-1)]^T$. Thus, the multivariate representation is defined by:

$$\begin{bmatrix} \mathbf{Y}_0 \\ \mathbf{Y}_1 \\ \vdots \\ \mathbf{Y}_N \end{bmatrix} = \begin{bmatrix} [\mathbf{y}_0^{(1)} \quad \mathbf{y}_0^{(2)} \quad \dots \quad \mathbf{y}_0^{(m)}]^T \\ [\mathbf{y}_1^{(1)} \quad \mathbf{y}_1^{(2)} \quad \dots \quad \mathbf{y}_1^{(m)}]^T \\ \vdots \\ [\mathbf{y}_{N-1}^{(1)} \quad \mathbf{y}_{N-1}^{(2)} \quad \dots \quad \mathbf{y}_{N-1}^{(m)}]^T \end{bmatrix} \quad (14)$$

Similar to (2), the input-output measurement pairs of an known input allow the output sequence for multiple channels to be expressed as:

$$\begin{cases} \mathbf{Y}_0 = \tilde{\mathbf{D}} \\ \mathbf{Y}_1 = \tilde{\mathbf{C}}\tilde{\mathbf{B}} \\ \mathbf{Y}_2 = \tilde{\mathbf{C}}\tilde{\mathbf{A}}\tilde{\mathbf{B}} \\ \vdots \\ \mathbf{Y}_{N-1} = \tilde{\mathbf{C}}\tilde{\mathbf{A}}^{N-1}\tilde{\mathbf{B}} \end{cases} \quad (15)$$

Notably, (15) follows the same sequence as (4) of the Markov parameters for multiple channels (named as $\tilde{\mathbf{A}}$, $\tilde{\mathbf{B}}$, $\tilde{\mathbf{C}}$, and $\tilde{\mathbf{D}}$). Consequently, (7) can also be expressed for multiple outputs channels as $\tilde{\mathbf{H}}(k) = \xi \tilde{\mathbf{A}}^{k-1} \tilde{\mathbf{B}}$. The block Hankel matrix in (8) is transformed into:

$$\tilde{\mathbf{H}}(k) = \begin{bmatrix} \mathbf{Y}_k & \mathbf{Y}_{k+1} & \dots & \mathbf{Y}_{k+N} \\ \mathbf{Y}_{k+1} & \mathbf{Y}_{k+2} & \dots & \mathbf{Y}_{k+N+1} \\ \vdots & \vdots & \ddots & \vdots \\ \mathbf{Y}_{k+N} & \mathbf{Y}_{k+N+1} & \dots & \mathbf{Y}_{k+2N} \end{bmatrix} \quad (16)$$

By assuming $k=1$ and $k=2$ in (16), Hankel matrices $\tilde{\mathbf{H}}(1)$ and $\tilde{\mathbf{H}}(2)$ can be derived using (10).

Then, $\tilde{\mathbf{B}}$ and $\tilde{\mathbf{A}}$ can be obtained from $\tilde{\mathbf{H}}(1) \in \mathbf{R}^{m(N/2-1) \times (N/2-1)}$ and $\tilde{\mathbf{H}}(2) \in \mathbf{R}^{m(N/2-1) \times (N/2-1)}$, respectively. Therefore, the Markov parameters for multiple output channels are:

$$\begin{cases} \tilde{\mathbf{A}} = \tilde{\mathbf{S}}^{-1/2} \tilde{\mathbf{P}}^T \tilde{\mathbf{H}}(2) \tilde{\mathbf{Q}} \tilde{\mathbf{S}}^{-1/2} \\ \tilde{\mathbf{B}} = \tilde{\mathbf{S}}^{1/2} \tilde{\mathbf{Q}}^T \\ \tilde{\mathbf{C}} = \tilde{\mathbf{P}} \tilde{\mathbf{S}}^{1/2} \\ \tilde{\mathbf{D}} = \mathbf{Y}_0 \end{cases} \quad (17)$$

III. SWITCHING MODEL AND FS-BASED GENERALIZED AVERAGE MODEL

The FS-based generalized average modeling is the most frequently used method for resonant and multi-resonant converters [4], [13], [21]. This renders the technique suitable for comparison with the ERA proposed in this paper. The generalized average modeling technique allows the characterization of the dynamic behavior of AC variables and the representation of any arbitrary types of waveforms as a sum of sinusoids. However, deriving the converter model using this technique requires extensive knowledge of the physical behavior of the circuit and exact converter parameter values; and considerable efforts of designer are also necessary. In this paper, the generalized average model is only used for comparison. Thus, this section details a switching model and general average model contingent on an FS representing a sliding window with a novel set of DAB converter state variables. In this case, the transformer current i_t and output capacitor voltage v_o are selected as state variables.

A simple phase-shift modulation (SPSM) scheme is adopted in this paper to control the power flow between the input and output terminals [36], [37]. Based on the operation principles of SPSM, the primary and secondary bridges are controlled by square-wave voltages with a 50% duty cycle and fixed frequency [14], [20]. The phase shift φ among the driving signals regulates the direction and magnitude of the power flowing through L_t between the input and output sides. The model is derived by assuming that the magnetizing transformer current is insignificant, the voltage drops across the switches and capacitor are negligible, and the switching transients are not detectable. Moreover, the input capacitance is relatively large; hence, the dynamics of the input capacitor are not considered. The switch gate signals over each bridge are displayed in Fig. 3, where T is the switching signal period.

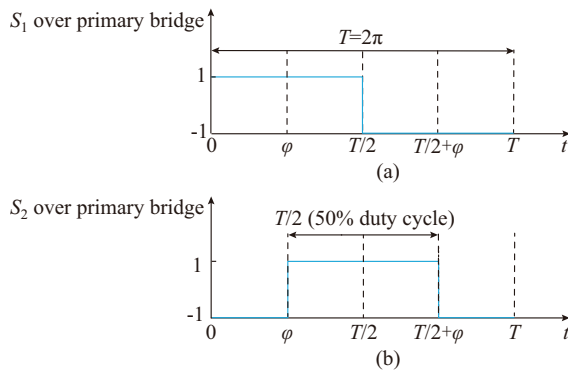


Fig. 3. Waveforms of switching functions S_1 and S_2 during one switching cycle. (a) S_1 . (b) S_2 .

The power transferred to both bridges is defined as [4], [5], [13], [14], [20]:

$$P = \frac{|v_i||v_o|}{2Nf_{sw}L_t} d(1-d) = \frac{|v_i||v_o|}{2\pi Nf_{sw}L_t} \varphi \frac{(\pi - \varphi)}{\pi} \quad (18)$$

where $f_{sw} = 1/T$ is the switching frequency; d is the phase shift ratio equal to φ/π ; and φ is the phase shift in radians.

The voltage at the input terminal (referred to the output terminal) is expressed as $v_p = v_s/N$. Using the SPSM, the voltage on the transformer input side v_p has two possible states: v_i when switches Q_1 and Q_2 are ON, and $-v_i$ when switches Q_3 and Q_4 are ON. The input terminal voltage v_p can be defined as:

$$v_p = S_1 v_i \quad (19)$$

where the switching function at the input terminal S_1 is given by:

$$S_1 = \begin{cases} 1 & 0 < t \leq \frac{T}{2} \\ -1 & \frac{T}{2} < t \leq T \end{cases} \quad (20)$$

At the output terminal, this becomes:

$$v_s = S_2 v_o \quad (21)$$

where the switching function at the output terminal S_2 is given by:

$$S_2 = \begin{cases} 1 & \varphi < t \leq \frac{T}{2} + \varphi \\ -1 & 0 < t \leq \varphi \text{ or } \frac{T}{2} + \varphi < t < T \end{cases} \quad (22)$$

Using Kirchhoff's laws and the state equations of DAB converter for switching, the time-varying and nonlinear model can be derived as:

$$C \frac{dv_o}{dt} = -\frac{v_o}{R} + S_2 \frac{i_t}{N} \quad (23)$$

$$L_t \frac{di_t}{dt} = -R_t i_t - S_2 \frac{v_o}{N} + S_1 v_i \quad (24)$$

where $i_t = N i_{t2}$; and $i_s = S_2 i_{t2} = S_2 i_t/N$.

The average method may be applied to derive a time-invariant model. It represents each state variable $x(\tau)$ by the real and imaginary coefficients of the FS for $t-T \leq \tau \leq t$ to obtain the switching moving average model [4]. The time-invariant model can be derived by applying the definition presented in (26) to average S_1 and S_2 within a commutation period T . Additionally, the parameters of DAB converter are assumed to be constants. In this way, the generalized average model is invariant in time, because it does not explicitly contain the variable t [13], [21].

The error between the switching model and average model can be reduced by increasing the value of the FS coefficient; however, this increases the complexity of the model, and no additional information for controller design or system-level analysis is obtained. In this paper, the coefficient $k=0, 1$, and -1 are studied.

$$x(\tau) = \sum_{k=-\infty}^{\infty} \langle x \rangle_k(t) e^{jk\omega_o\tau} \quad (25)$$

where $\omega_o = 2\pi f_{sw} = 2\pi/T$; and $\langle x \rangle_k(t)$ is the k^{th} complex FS decomposed into real and imaginary components in continuous time, given by:

$$\langle x \rangle_k(t) = \frac{1}{T} \int_{t-T}^t x(\tau) (\cos(k\omega_o\tau) - j\sin(k\omega_o\tau)) d\tau \quad (26)$$

The DC term $\langle x \rangle_0(t)$ denoting the average value of signal $x(\tau)$ in (26) can be deduced by setting $\omega_o = 0$ in (26).

The DAB converter described by (23) and (24) can be expressed in terms of its Fourier coefficients using the time-derivative of the k^{th} coefficient for variable x and the properties of Fourier coefficients [13], [21]. The DC component ($k=0$) of v_o is defined by (27), and its real and imaginary parts are established by (28) and (29), respectively.

$$\frac{d}{dt}\langle v_o \rangle_o = -\frac{\langle v_o \rangle_o}{RC} + \frac{\langle S_2 \rangle_o \langle i_t \rangle_o}{C} + \frac{2}{C} \left(\langle S_2 \rangle_{1R} \langle i_t \rangle_{1R} + \langle S_2 \rangle_{1I} \langle i_t \rangle_{1I} \right) \quad (27)$$

$$\frac{d}{dt}\langle v_o \rangle_{1R} = -\frac{1}{RC}\langle v_o \rangle_{1R} + \omega_o \langle v_o \rangle_{1I} + \frac{1}{C} \langle S_2 \rangle_o \langle i_t \rangle_{1R} + \frac{1}{C} \langle S_2 \rangle_{1R} \langle i_t \rangle_o \quad (28)$$

$$\frac{d}{dt}\langle v_o \rangle_{1I} = -\frac{1}{RC}\langle v_o \rangle_{1I} - \omega_o \langle v_o \rangle_{1R} + \frac{1}{C} \langle S_2 \rangle_o \langle i_t \rangle_{1I} + \frac{1}{C} \langle S_2 \rangle_{1I} \langle i_t \rangle_o \quad (29)$$

The zero and first harmonic components of the transformer current are derived as (30)-(32).

$$L_t \frac{d}{dt} \langle i_t \rangle_o = -R_t \langle i_t \rangle_o - \frac{1}{N} \left(\langle S_2 \rangle_o \langle v_o \rangle_o + 2 \langle S_2 \rangle_{1R} \langle v_o \rangle_{1R} + 2 \langle S_2 \rangle_{1I} \langle v_o \rangle_{1I} \right) + \langle S_1 \rangle_o \langle v_i \rangle_o + 2 \langle S_1 \rangle_{1R} \langle v_o \rangle_{1R} + 2 \langle S_1 \rangle_{1I} \langle v_o \rangle_{1I} \quad (30)$$

$$L_t \frac{d}{dt} \langle i_t \rangle_{1R} = -R_t \langle i_t \rangle_{1R} + \omega_o \langle i_t \rangle_{1I} - \frac{1}{N} \left(\langle S_2 \rangle_o \langle v_o \rangle_{1R} + \langle S_2 \rangle_{1R} \langle v_o \rangle_o \right) + \langle S_1 \rangle_o \langle v_i \rangle_{1R} + \langle S_1 \rangle_{1R} \langle v_i \rangle_o \quad (31)$$

$$L_t \frac{d}{dt} \langle i_t \rangle_{1I} = -R_t \langle i_t \rangle_{1I} - \omega_o \langle i_t \rangle_{1R} - \frac{1}{N} \left(\langle S_2 \rangle_o \langle v_o \rangle_{1I} + \langle S_2 \rangle_{1I} \langle v_o \rangle_o \right) + \langle S_1 \rangle_o \langle v_i \rangle_{1I} + \langle S_1 \rangle_{1I} \langle v_i \rangle_o \quad (32)$$

The k^{th} coefficient of the FS for switching signals S_1 and S_2 are derived by substituting (20) and (22) into (26). The signals S_1 and S_2 are symmetric and only have the AC component by assuming a 50% duty cycle, i.e., its DC component can be calculated in such a way that $\langle S_1 \rangle_o = \langle S_2 \rangle_o = 0$.

Thus, the real and imaginary components for the first coefficient values of $\langle S_1 \rangle$ and $\langle S_2 \rangle$ can be derived as:

$$\begin{cases} \langle S_1 \rangle_{1R} = 0 \\ \langle S_1 \rangle_{1I} = -\frac{2}{\pi} \end{cases} \quad (33)$$

$$\begin{cases} \langle S_2 \rangle_{1R} = -\frac{2\sin\varphi}{\pi} \\ \langle S_2 \rangle_{1I} = -\frac{2\cos\varphi}{\pi} \end{cases} \quad (34)$$

The dynamics of v_o and v_i may be assumed to be extremely slower compared with the other dynamics; thus, $v_o = V_o + V_{\text{Ripple}}$, where V_o is the output voltage in RMS and V_{Ripple} is the ripple of the output voltage, such that $|V_{\text{Ripple}}| \ll V_o$. Consequently, this paper assumes that $\langle v_o \rangle_{1R} = \langle v_o \rangle_{1I} = \langle v_i \rangle_{1R} =$

$\langle v_i \rangle_{1I} = 0$. Hence, v_o and v_i can be expressed as V_o and V_i using only the DC component, respectively. The transformer current only has AC components, i.e., $\langle i_t \rangle_o = 0$. Based on the foregoing assumptions and substituting (33), (34) into (27)-(32), the generalized average model of DAB is derived in matrix form as:

$$\frac{d}{dt} \begin{bmatrix} V_o \\ \langle i_t \rangle_{1R} \\ \langle i_t \rangle_{1I} \end{bmatrix} = \begin{bmatrix} -\frac{1}{RC} & -\frac{4\sin\varphi}{C\pi} & -\frac{4\cos\varphi}{C\pi} \\ \frac{2\sin\varphi}{N\pi L_t} & -\frac{R_t}{L_t} & \frac{\omega_o}{L_t} \\ \frac{2\cos\varphi}{N\pi L_t} & -\frac{\omega_o}{L_t} & -\frac{R_t}{L_t} \end{bmatrix} \begin{bmatrix} V_o \\ \langle i_t \rangle_{1R} \\ \langle i_t \rangle_{1I} \end{bmatrix} + \begin{bmatrix} 0 \\ 0 \\ \frac{2}{\pi L_t} \end{bmatrix} V_i \quad (35)$$

The straightforward implementation of the DAB average model, derived by FS analysis, can be achieved by embedding the differential equation in (35) on a MATLAB function in Simulink. Moreover, the parameters and an integration loop have to be defined, as shown in Fig. 4.

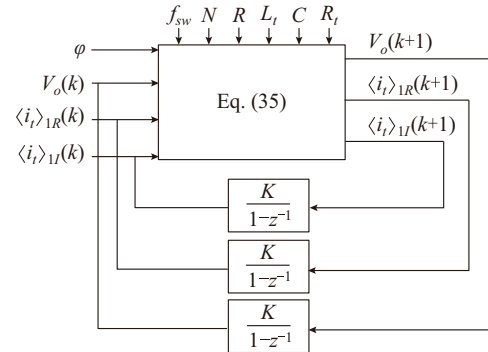


Fig. 4. Averaged model implementation by FS.

IV. EXPERIMENTAL TESTS AND SIMULATION RESULTS

This section presents the experimental tests and simulation results of the proposed ERA model applied to the DAB converter under both transient and steady-state conditions. Several comparisons are implemented to verify the effectiveness of the ERA modeling method and precisely identify the dynamic behavior of power electronic converters with a substantially reduced computation time. The time response of the ERA model is compared with those derived from the DAB experimental measurements, DAB switched circuit (SC) model, and FS-based generalized average model. The data used to identify the system are gathered with respect to the response of the system to a step signal from 0° to 90° in φ in two scenarios: ① using measurements from the DAB SC simulation; and ② using the measurements at the input and output ports of the actual DAB prototype. The simulations are executed using the MATLAB/Simulink software. Meanwhile, the DAB prototype is hardware-implemented.

To practically validate the proposed method for modeling

the DAB converter, experiments are conducted on an actual DAB prototype. The simulation and experimental parameters of the electronic converter shown in Figs. 2 and 5 are listed in Table II.

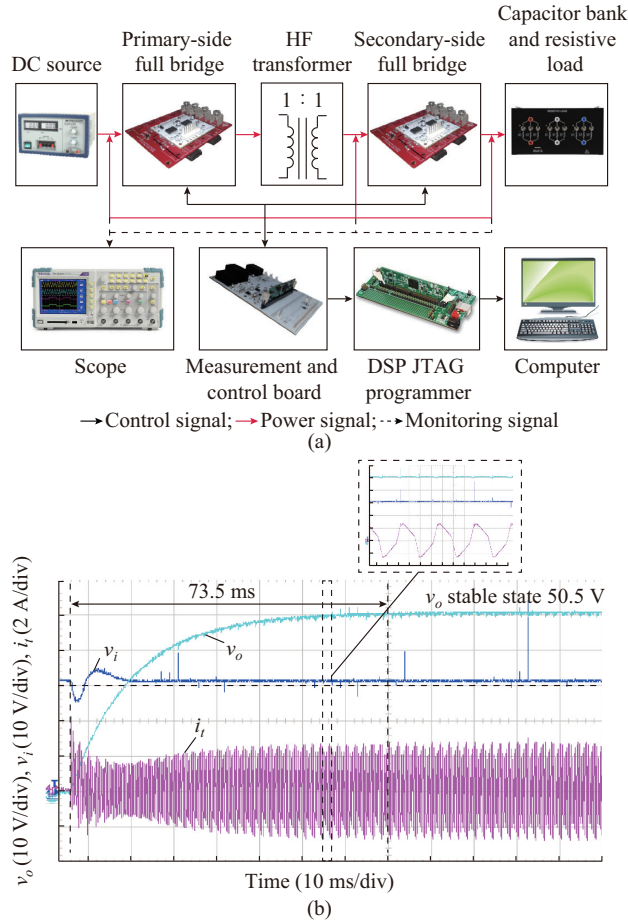


Fig. 5. Experimental setup. (a) DAB prototype. (b) Dynamic response of v_o , v_i , and i_t when ϕ changes from 0° to 90° in step shape.

TABLE II

SIMULATION AND EXPERIMENTAL PARAMETERS

Parameter	Value
Load resistor R	53.4 Ω
DC bus capacitor C	340 μF
DC input voltage v_i	31 V
DAB leakage inductance L_t	1.02 mH
DAB transformer ratio	1:1
DAB switching frequency f_{sw}	3000 Hz
Sample time	1 μs
Phase shift ϕ	0° - 90°

The measurements of v_i , v_o , and i_t are monitored by the test probes in the DAB prototype. They are recorded via the DSO4048C scope at a sampling rate of 1 MHz. The sampling rate of electrical signals must be uniform and exceed the highest frequency of the signal by at least a factor of two to be retained in the model. However, the minimum sampling frequency is recommended to be at least 10 times higher than the maximum frequency of the measured vari-

able [38].

The SPS modulation strategy and the proportional-integral (PI) controller are implemented using the F28335 digital signal processor (Texas Instrument) and a self-powered control board. The embedded software is completely developed in C, and its online coding is available in [39]. The active bridges are formed by eight TP65H035WSQA GaN power switches, each equipped with integrated anti-parallel diode, isolated drivers, and sources. The real DAB prototype is implemented with independent functional modules, as presented in Fig. 5(a).

In the open-loop experimental results, v_o increases up to 50.5 V at 73.5 ms due to the change in ϕ from 0° to 90° . When the step-change occurs, a slight oscillation is observed in the input voltage caused by the rapid absorption of the current from L_t and C . The surge in the transformer current i_t in the steady state exhibits the typical waveform for $v_o > v_i$.

The straightforward implementation of ERA described in Section II proceeds by eliminating the voltage and transformer current signals obtained from the actual data at a 1 MHz sampling rate by a factor of 40. This enables the attainment of a frequency rate reduction of up to 25 kHz.

Two criteria are established for selecting the correct order of the ERA model: ① the total energy of the singular values for matrix $\mathbf{H}(l)$; and ② the magnitude of the first singular values for $\mathbf{H}(l)$, as illustrated in Fig. 6(a) and (b), respectively. The former criterion derives the 12th-order ERA (12ERA) model, which is achieved by assigning 71.33% of the total system energy. However, the reduction in the order of the ERA model is realized by comparing the magnitudes of the first singular values of matrix $\mathbf{H}(l)$. Notably, in Fig. 6(b), the first four values significantly exceed the magnitudes of the following singular values, resulting in the 4th-order ERA (4ERA) model, which is selected for comparison in this paper. Appendix A presents the system identification of the 12ERA and 4ERA models.

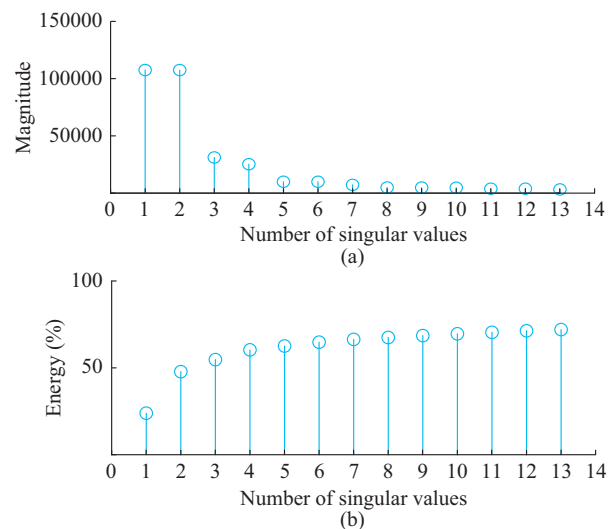


Fig. 6. Magnitudes of first singular values and their energies for $\mathbf{H}(l)$. (a) Magnitude. (b) Energy.

The time-domain results of the output voltage v_o and leak-

age transformer current i_l for the 4ERA, 12ERA, FS, and SC models as well as for the experimental measurements are illustrated in Fig. 7. The actual measurements are assumed as a base for comparison. Figure 7(a) indicates that the output voltage is consistent in both transient and steady-state responses with an approximate settling time of 73 ms for all compared models. The transient response of all models in this plot matches the similar behavior of the prototype. Figure 7(b) shows the leakage transformer current i_l for the 4ERA, 12ERA, FS, and SC models, and the experimental measurements. Notice that i_l only has AC components, and the 4ERA, 12ERA, and FS models can describe the magnitude and temporal evolution of the transformer current in contrast with the experimental measurements. In this test, the output results predicted by the FS model are only sinusoidal approximations of the current. This is because the FS model only considers the sum of sinusoids in the FS with $k=0, 1, \text{ and } -1$. The transformer current achieved by the 4ERA model also has a pure sine waveform; nevertheless, this model allows gaining a better approximation of the average current value. By contrast, the 12ERA model approximation of the transformer current waveform is considerably superior to those of the other models. The results demonstrate the accuracy of the DAB dynamic modeling driven by both the 4ERA and 12ERA models.

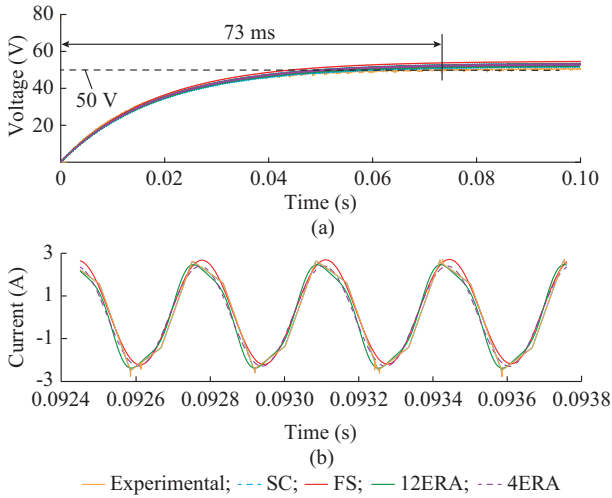


Fig. 7. Waveforms of 4ERA, 12ERA, FS, SC models and experimental measurements. (a) Output voltage v_o . (b) Zoom of leakage inductance current i_l .

The reduction in the computational effort that the ERA model affords is shown in Fig. 8. The summary of the Simulink profile report under the same simulation conditions is utilized to obtain the simulation metrics; each model is simulated 100 times with a sampling time of 1 μs . The computer system has a 2.1 GHz AMD Razor 5 processor, 20 GB RAM and 64-bit WIN10 operation system. The simulation time data are used to construct the statistical report presented in Fig. 8. For each model, \bar{x} and σ are the mean and standard deviations of the simulation time, respectively. The report highlights that the ERA model runs 8.55 and 1.51 times faster than the FS and SC models, respectively.

The SC, FS, 4ERA, and 12ERA models as well as the fre-

quency spectra from the experimental measurements validate the frequency content in the output voltage and transformer current channels, as shown in Fig. 9(a) and (b), respectively. In contrast with the experimental measurements, the analyzed models exhibit a close harmonic content. The frequency spectra of the output voltage v_o devote a considerable amount of energy to the frequency components approaching 0 Hz and a small spectral content at the switching frequency and its harmonics. On the contrary, the frequency spectra of the transformer current models present the highest amount of energy at the switching frequency of 3 kHz and its harmonics.

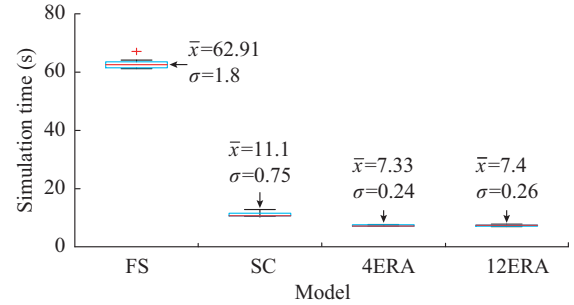


Fig. 8. Box plot of simulation time.

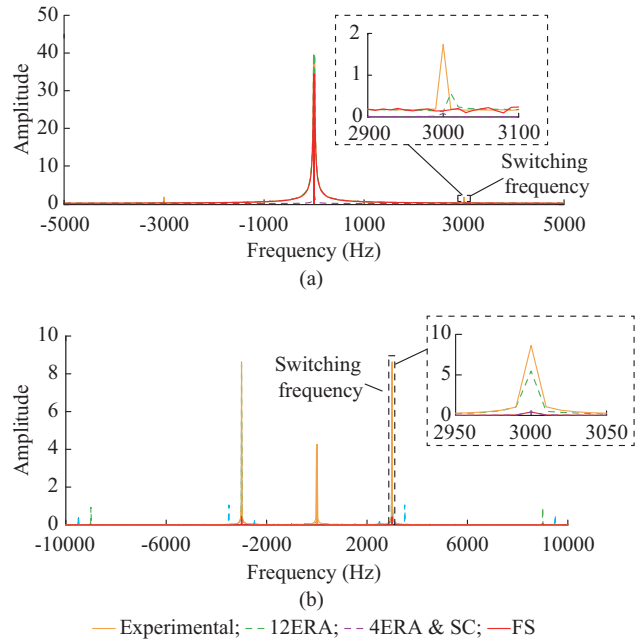


Fig. 9. SC, FS, 4ERA, 12ERA models and frequency spectra from experimental measurements. (a) v_o . (b) i_l .

The steady-state performance is evaluated for the FS model and the 4ERA and 12ERA models through the frequency response using the Bode diagrams, as depicted in Fig. 10. Note that the models are similar in terms of magnitude and phase; however, the 12ERA model represents the switching frequency and its similar harmonics in greater detail.

Figures 11 and 12 depict the RMSE simulation results and signal-to-noise ratio (SNR) metrics between the FS, 4ERA, and 12ERA models compared with the SC model. The error metrics between the calculated models and the reference sig-

nal allow the quantitative comparison of the precision of the proposed ERA model with other models and reference signal. An SNR of 31 dB for the 12ERA model indicates that the approximation error energy is up to 1000 times smaller than that of the switched model, indicating a suitable match among the models. In contrast, the approximation error energy for the FS and 4ERA models is only 10 times smaller. For the RMSE, the smallest values are attained by the 12ERA model in both voltage and current channels.

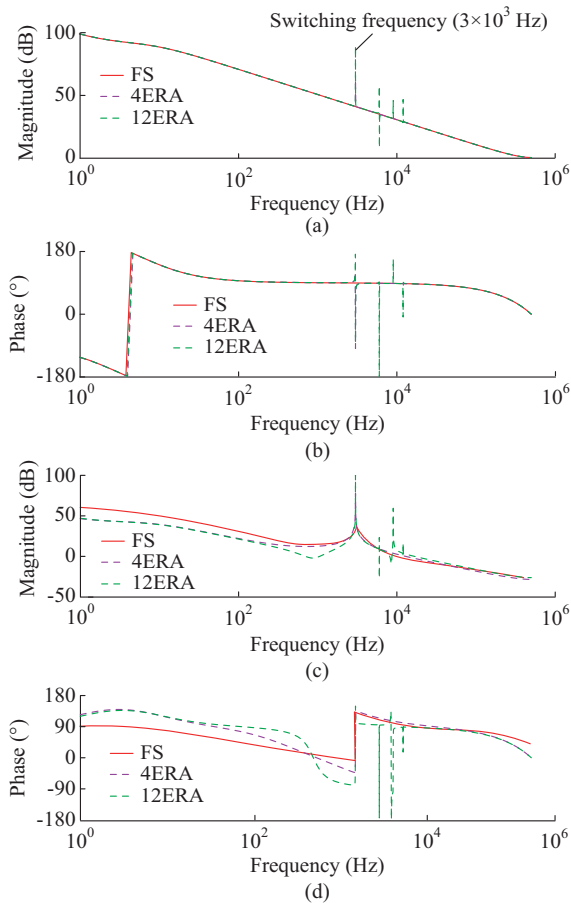


Fig. 10. Bode diagrams for 4ERA and 12ERA models in comparison with FS model. (a) Output voltage v_o . (b) Input phase ϕ for transfer function ($|V_o(s)/\Phi(s)|$). (c) Output transformer current i_r . (d) Input phase ϕ for transfer function ($|I_r(s)/\Phi(s)|$).

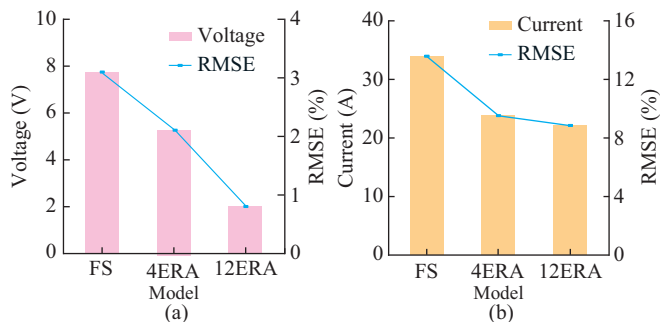


Fig. 11. Comparison of RMSE between FS and ERA models. (a) v_o . (b) i_r .

A comparison between the identified 12ERA model response and actual converter response is shown in Fig. 13 when the input phase ϕ is perturbed and the input voltage is

kept constant. This perturbation is introduced by two step-up phases: ① from 0° to 45° ; and ② from 45° to 90° . Under these conditions, 70 ms elapse before the model and actual converter reach the settling time. Figure 13 indicates that both responses are extremely similar; hence, the output voltage of the converter has been properly modeled. The proposed model can be used to predict the performance of converter in similar scenarios in which the model is computed.

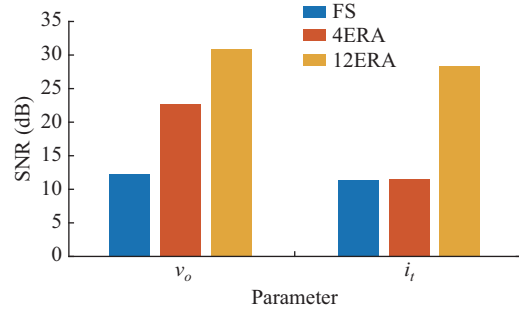


Fig. 12. Comparison of SNR between FS and ERA models.

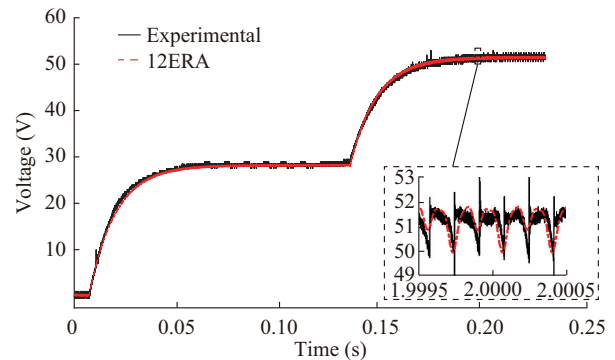


Fig. 13. Comparison between actual measured response and prediction of 12ERA model when perturbations of input phase ϕ are applied.

The ERA model can be applied with low computational effort to simulate the system level in electrical networks with a high penetration of electronic converters or to tune power circuit controllers, as detailed in Fig. 14.

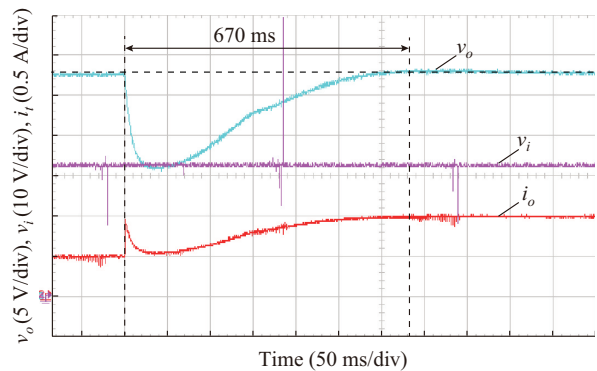


Fig. 14. Closed-loop performance with PI controller tuned with 12ERA model.

The 12ERA model is employed to tune the PI controller through the root geometric place methodology to increase the robustness of the system in the presence of significant load changes. The computed parameters for the controller

are $k_p=3.8\times 10^{-3}$ and $k_i=0.5\times 10^{-3}$. The controller performance is verified by applying a 100% step load increase, resulting in a 12 V voltage drop and allowing 670 ms to elapse before returning to the steady-state condition. Although the closed-loop system is tuned to operate with respect to an operating point, the controller parameters enable the system to function under extreme conditions with acceptable results, evincing the applicability of the proposed modeling technique.

V. CONCLUSION

Simplified models are particularly essential system-level representations for balancing accuracy and complexity in the analysis and simulation of systems highly interfaced with power electronic converters. This guarantees the trade-off between the precision and the level of detail required for analysis. In such a context, the systematic procedure presented in this paper can construct scalable models at the system level with a reasonable computational cost.

The proposed modeling approach driven by the eigensystem realization is compatible with the system-level analysis approaches typically applied to large-scale power systems. Although this paper is focused on the system identification framework for DAB converters, the modeling procedure can be applied to any converter topology with considerable precision, representing the switched-mode analysis with sufficient details. Such simplicity of the proposed method renders it accessible to the power system and power electronic engineers.

Via the ERA, this paper has also demonstrated that a dynamic model based on the optimal energy reduction for the

DAB converter from the measured response can be feasibly derived. After assessing the ERA-based DAB model under steady-state and dynamic conditions, appropriate modeling with sufficient precision can be ensured. The identified system captures the maximum energy represented by the higher singular values corresponding to the highest energy of the physical system.

Given the multiple outputs of ERA-based modeling, the observability of the physical system can be attained, allowing its identification with any phase perturbations in the DAB phase-shift modulation.

The results indicate that the proposed DAB model, given its adaptability, can track changes in voltage and current ripples even under noisy conditions. It has the capacity to excite and render all system frequencies evident, allowing the capture of the system modal information. This method significantly improves the accuracy of the transformer current model, which is absent from the DAB models derived using the FS. Accordingly, the eigensystem realization driven approach is regarded as an emerging powerful and reliable tool for power electronic converter modeling.

APPENDIX A

Appendix A presents the system identification. For the identified 12ERA model of the DAB, the Markov parameters in continuous-time are given by (A1). These are obtained after applying the MATLAB function *d2c* to the discrete-time system in (17). In the same way, the state-space model for the identified 4ERA model is represented by (A2).

$$\begin{aligned} \tilde{\mathbf{A}} &= \begin{bmatrix} 9.157 & 24.03 & 0.1654 & 0.645 & -0.051 & 1.955 & -0.188 & 0.083 & -0.01 & -0.186 & 0.032 & 1.05 \\ 24.09 & -63.39 & 35.35 & 0.613 & -3.173 & 29.86 & -3.279 & 2.711 & 1.30 & -1.472 & 0.519 & 14.63 \\ 3.027 & -78.69 & 6.282 & 18854 & 0.138 & -0.746 & -6.192 & 3.891 & 25.54 & 28.004 & -0.039 & 0.772 \\ -2.86 & 26.06 & -18854 & 6.193 & 0.040 & 3.82 & -4.19 & 5.827 & 12.01 & 10.41 & 0.068 & 0.875 \\ 0.016 & -2.498 & -0.488 & -0.541 & -1.025 & -37700 & 0.807 & -1.4365 & -3.952 & 1.904 & 2.69 & -0.582 \\ 1.956 & -29.97 & 10.28 & -10.18 & 37700 & 19.08 & -27.24 & -17.28 & -29.695 & 27.50 & 0.57 & 27.24 \\ 1.001 & -10.15 & 6.184 & -4.20 & -1.439 & 36.69 & 6.75 & -56543.3 & -109.15 & -18.86 & 1.095 & 3.690 \\ 1.007 & -22.32 & 3.88 & -5.97 & 1.82 & 30.45 & 56543.25 & 5.41 & 49.44 & 212.74 & -0.7008 & 9.596 \\ 3.690 & 19.31 & 27.03 & -12.26 & 9.847 & 82.91 & 111.38 & 57.65 & -57.65 & -18846.7 & -10.95 & 110.77 \\ -3.36 & -20.05 & -28.15 & 10.20 & -5.391 & -76.108 & -23.18 & -212.5 & 18846 & -63.17 & -0.737 & -104.37 \\ 0.032 & -0.807 & -0.115 & -0.460 & -2.718 & 0.526 & -2.35 & 3.15 & 16.68 & 0.49 & -4.558 & 75398 \\ -1.052 & 14.64 & -5.48 & 5.035 & -0.14 & -27.18 & -18.22 & -20.4 & -169.47 & 157.8 & -75398.3 & 22.5 \end{bmatrix} \\ \tilde{\mathbf{B}} &= [-245000 \quad -243665 \quad -67712 \quad 20762.3 \quad -3246.7 \quad -26378.6 \quad -8567.4 \quad -23134 \quad 38485.7 \quad -38112.9 \quad -849.3 \quad 13984.5]^T \\ \tilde{\mathbf{C}} &= \begin{bmatrix} -4.892 & 4.866 & -0.0752 & -0.2329 & -0.1183 & -0.504 & 0.04231 & -0.0697 & -0.0409 & 0.0364 & 0.1673 & -0.19109 \\ -0.2997 & -0.1009 & 1.2165 & 0.6625 & -0.0057 & -0.0113 & 0.1076 & 0.448 & -0.882 & -0.604 & 0.004 & -0.0063 \end{bmatrix} \end{aligned} \quad (\text{A1})$$

$$\begin{aligned} \tilde{\mathbf{A}} &= \begin{bmatrix} 9.157 & 24.035 & 0.165 & 0.645 \\ -24.096 & -63.405 & 35.35 & 0.610 \\ 3.028 & -78.69 & 6.283 & 18854 \\ -2.859 & 26.05 & -18854 & 6.192 \end{bmatrix} \\ \tilde{\mathbf{B}} &= [-245000 \quad -243671 \quad -67711 \quad 20761]^T \\ \tilde{\mathbf{C}} &= \begin{bmatrix} -4.8926 & 4.8665 & -0.0752 & -0.2329 \\ -0.2997 & -0.1009 & 1.2165 & 0.6625 \end{bmatrix} \end{aligned} \quad (\text{A2})$$

REFERENCES

- [1] A. Elserougi, I. Abdelsalam, A. Massoud *et al.*, "A non-isolated hybrid-modular DC-DC converter for DC grids: small-signal modeling and control," *IEEE Access*, vol. 7, pp. 132459-132471, Sept. 2019.
- [2] G. San, W. Zhang, R. Luo *et al.*, "Small-signal multi-frequency model for grid-connected inverter system with PWM effect," *CSEE Journal of Power and Energy Systems*, vol. 6, no. 2, pp. 307-317, Jun. 2020.
- [3] W. Liu, X. Xie, J. Shair *et al.*, "A nearly decoupled admittance model for grid-tied VSCs under variable operating conditions," *IEEE Transactions on Power Electronics*, vol. 35, no. 9, pp. 9380-9389, Sept. 2020.

- [4] S. R. Sanders, J. M. Noworolski, X. Liu *et al.*, "Generalized averaging method for power conversion circuits," *IEEE Transactions on Power Electronics*, vol. 6, no. 2, pp. 251-259, Apr. 1991.
- [5] S. S. Shah and S. Bhattacharya, "A simple unified model for generic operation of dual active bridge converter," *IEEE Transactions on Industrial Electronics*, vol. 66, no. 5, pp. 3486-3495, May 2019.
- [6] V. Valdivia, A. Barrado, A. Lazaro *et al.*, "Black-box behavioral modeling and identification of DC-DC converters with input current control for fuel cell power conditioning," *IEEE Transactions on Industrial Electronics*, vol. 61, no. 4, pp. 1891-1903, Apr. 2014.
- [7] A. Zamora-Mendez, F. Zelaya-A., J. de la O. Serna *et al.*, "Model-based synchrophasor estimation by exploiting the eigensystem realization approach," *Electric Power Systems Research*, vol. 182, p. 106249, May 2020.
- [8] O. Loyola-González, "Black-box vs. white-box: understanding their advantages and weaknesses from a practical point of view," *IEEE Access*, vol. 7, pp. 154096-154113, Oct. 2019.
- [9] V. Valdivia, A. Barrado, A. Lazaro *et al.*, "Simple modeling and identification procedures for 'black-box' behavioral modeling of power converters based on transient response analysis," *IEEE Transactions on Power Electronics*, vol. 24, no. 12, pp. 2776-2790, Dec. 2009.
- [10] C. Raga, A. Barrado, A. Lázaro *et al.*, "Black-box model, identification technique and frequency analysis for pem fuel cell with overshooted transient response," *IEEE Transactions on Power Electronics*, vol. 29, no. 10, pp. 5334-5346, Oct. 2014.
- [11] M. Klatt, R. Stiegler, J. Meyer *et al.*, "Generic frequency-domain model for the emission of PWM-based power converters in the frequency range from 2 to 150 kHz," *IET Generation, Transmission & Distribution*, vol. 13, no. 24, pp. 5478-5486, Dec. 2019.
- [12] G. Mejia-Ruiz, N. Munoz-Galeano, and J. Lopez-Lezama, "Modeling and development of a bridgeless PFC boost rectifier," *Revista Facultad de Ingenieria*, vol. 82, pp. 9-21, Mar. 2017.
- [13] J. A. Mueller and J. W. Kimball, "An improved generalized average model of DC-DC dual active bridge converters," *IEEE Transactions on Power Electronics*, vol. 33, no. 11, pp. 9975-9988, Nov. 2018.
- [14] J. A. Mueller and J. W. Kimball, "Modeling dual active bridge converters in DC distribution systems," *IEEE Transactions on Power Electronics*, vol. 34, no. 6, pp. 5867-5879, Jun. 2019.
- [15] G. Chen, L. Mo, Y. Liu *et al.*, "Computer-aided identification of equivalent power electronics converters," *IEEE Transactions on Power Electronics*, vol. 34, no. 10, pp. 9374-9378, Oct. 2019.
- [16] J. Poon, P. Jain, I. C. Konstantakopoulos *et al.*, "Model-based fault detection and identification for switching power converters," *IEEE Transactions on Power Electronics*, vol. 32, no. 2, pp. 1419-1430, Feb. 2017.
- [17] J.-Y. Choi, B. H. Cho, H. F. Van Landingham *et al.*, "System identification of power converters based on a black-box approach," *IEEE Transactions on Circuits and Systems I: Fundamental Theory and Applications*, vol. 45, no. 11, pp. 1148-1158, Nov. 1998.
- [18] S. Lee, Y. Jeung, and D. Lee, "Voltage balancing control of IPOS modular dual active bridge DC/DC converters based on hierarchical sliding mode control," *IEEE Access*, vol. 7, pp. 9989-9997, Jan. 2019.
- [19] Y. Jeung and D. Lee, "Voltage and current regulations of bidirectional isolated dual-active-bridge DC-DC converters based on a double-integral sliding mode control," *IEEE Transactions on Power Electronics*, vol. 34, no. 7, pp. 6937-6946, Jul. 2019.
- [20] K. Zhang, Z. Shan, and J. Jatskevich, "Large- and small-signal average-value modeling of dual-active-bridge DC-DC converter considering power losses," *IEEE Transactions on Power Electronics*, vol. 32, no. 3, pp. 1964-1974, Mar. 2017.
- [21] H. Qin and J. W. Kimball, "Generalized average modeling of dual active bridge DC-DC converter," *IEEE Transactions on Power Electronics*, vol. 27, no. 4, pp. 2078-2084, Apr. 2012.
- [22] M. Berger, I. Kocar, H. Fortin-Blanchette *et al.*, "Hybrid average modeling of three-phase dual active bridge converters for stability analysis," *IEEE Transactions on Power Delivery*, vol. 33, no. 4, pp. 2020-2029, Aug. 2018.
- [23] F. Zhang, M. M. U. Rehman, R. Zane *et al.*, "Improved steady-state model of the dual-active-bridge converter," in *Proceedings of 2015 IEEE Energy Conversion Congress and Exposition (ECCE)*, Montreal, Canada, Sept. 2015, pp. 630-636.
- [24] G. G. Oggier, M. Ordonez, J. M. Galvez *et al.*, "Fast transient boundary control and steady-state operation of the dual active bridge converter using the natural switching surface," *IEEE Transactions on Power Electronics*, vol. 29, no. 2, pp. 946-957, Feb. 2014.
- [25] Y. Yan, H. Bai, A. Foote *et al.*, "Securing full-power-range zero-voltage switching in both steady-state and transient operations for a dual-active-bridge-based bidirectional electric vehicle charger," *IEEE Transactions on Power Electronics*, vol. 35, no. 7, pp. 7506-7519, Jul. 2020.
- [26] L. Shi, W. Lei, Z. Li *et al.*, "Bilinear discrete-time modeling and stability analysis of the digitally controlled dual active bridge converter," *IEEE Transactions on Power Electronics*, vol. 32, no. 11, pp. 8787-8799, Nov. 2017.
- [27] G. Gao, W. Lei, Q. Tang *et al.*, "Decomposed discrete-time model and multiscale oscillations analysis of the DAB converter," *IEEE Transactions on Power Electronics*, vol. 35, no. 9, pp. 9133-9150, Sept. 2020.
- [28] L. Chen, L. Lin, S. Shao *et al.*, "Moving discretized control set model-predictive control for dual-active bridge with the triple-phase shift," *IEEE Transactions on Power Electronics*, vol. 35, no. 8, pp. 8624-8637, Aug. 2020.
- [29] H. Shi, K. Sun, H. Wu *et al.*, "A unified state-space modeling method for a phase-shift controlled bidirectional dual-active half-bridge converter," *IEEE Transactions on Power Electronics*, vol. 35, no. 3, pp. 3254-3265, Mar. 2020.
- [30] H. Shi, K. Sun, H. Wu *et al.*, "Unified state-space modeling method for dual-active-bridge converters considering bidirectional phase shift," in *Proceedings of 2018 IEEE Energy Conversion Congress and Exposition*, Portland, USA, Sept. 2018, pp. 643-649.
- [31] J. N. Juang and R. Pappa, "An eigensystem realization algorithm for modal parameter identification and model reduction," *Journal of Guidance, Control, and Dynamics*, vol. 8, no. 5, pp. 620-627, Sept. 1985.
- [32] I. Kamwa, R. Grondin, E. J. Dickinson *et al.*, "A minimal realization approach to reduced-order modeling and modal analysis for power systems response signals," *IEEE Transactions on Power Systems*, vol. 8, no. 3, pp. 1020-1029, Aug. 1993.
- [33] J. Sanchez-Gasca and D. Trudnowski, "Identification of electromechanical modes in power system," IEEE Task Force on Identification of Electromechanical Modes of the Power System Stability, Tech. Rep., Jun. 2012.
- [34] J. de la O. Serna, J. Ramirez, A. Z. Mendez *et al.*, "Identification of electromechanical modes based on the digital Taylor-Fourier transform," *IEEE Transactions on Power Systems*, vol. 31, no. 1, pp. 206-215, Jan. 2016.
- [35] J. Bay, *Fundamentals of Linear State Space Systems*. New York: WCB/McGraw-Hill, 1999.
- [36] H. Shi, H. Wen, and Y. Hu, "Deadband effect and accurate ZVS boundaries of gan-based dual-active-bridge converters with multiple-phase-shift control," *IEEE Transactions on Power Electronics*, vol. 35, no. 9, pp. 9888-9905, Sept. 2020.
- [37] Y. Liu, X. Wang, W. Qian *et al.*, "A simple phase-shift modulation using parabolic carrier for dual active bridge DC-DC converter," *IEEE Transactions on Power Electronics*, vol. 35, no. 8, pp. 7729-7734, Aug. 2020.
- [38] N. Fu, X. Wei, L. Qiao *et al.*, "Short-observation measurement of multiple sinusoids with multichannel sub-Nyquist sampling," *IEEE Transactions on Instrumentation and Measurement*, vol. 69, no. 9, pp. 6853-6869, Sept. 2020.
- [39] G. E. Mejia-Ruiz, M. Paternina, J. Rodriguez *et al.* (2021, Jan.). Eigensystem realization algorithm-based dual active bridge model. [Online]. Available: https://github.com/gemejiar/DAB_ERA_control

Gabriel Mejia-Ruiz received the B.Eng. degree in control engineering from National University of Colombia, Medellin, Colombia, in 2007, and the M.Eng. degree in electrical engineering from Antioquia State University, Medellin, Colombia, in 2014. Since 2020, he is pursuing his Ph.D. degree in electrical engineering at National Autonomous University of Mexico (UNAM), Mexico City, Mexico. His research interests include power electronics converter, grid integration, and active and reactive control in distribution network.

Mario R. A. Paternina received the B.Eng. and M.Eng. degrees in electrical engineering from National University of Colombia, Medellin, Colombia, in 2007 and 2009, respectively. He received his D.Sc. degree in electrical engineering from Center for Research and Advanced Studies (CINVESTAV, in Spanish), Guadalajara, Mexico, in 2017. He joined the Department of Electrical Engineering at National Autonomous University of Mexico (UNAM), Mexico City, Mexico, in 2017. He was a Visiting Scholar at Rensselaer Polytechnic Institute in 2016. His research interests include model reduction, coherency, wide-area monitoring, protection and control system, and dynamic performance of power system.

Juan R. Rodriguez R. received the B.Eng. and Ph.D. degrees in electrical

engineering from the Morelia Institute of Technology, Morelia, Mexico, in 2009 and 2015, respectively. He is currently an Associate Professor at the Department of Electrical Energy, National Autonomous University of Mexico (UNAM), Mexico City, Mexico. His current research interests include power electronics converter, smart grid, and renewable energy.

Juan M. Ramirez received the Ph.D. degree in electrical engineering from Universidad Autónoma de Nuevo León, San Nicolas de los Garza, Mexico, in 1992. He joined the Department of Electrical Engineering, Center for Research and Advanced Studies (CINVESTAV), Guadalajara, Mexico, in 1999, where he is currently a Full-time Professor. His research interests include smart grid, microgrid, and power electronics application.

Alejandro Zamora-Mendez received the B.S. and M.Sc. degrees in electrical engineering from Michoacan University of Saint Nicholas of Hidalgo (UMSNH), Morelia, Mexico, in 2005 and 2008, respectively. In 2016, he re-

ceived his D.Sc. degree in electrical engineering from Center for Research and Advanced Studies (CINVESTAV), Guadalajara, Mexico. He joined the Electrical Engineering Faculty, UMSNH, in 2008, where he is a Full-time Professor. He was a Visiting Scholar at Washington State University, Pullman, USA, in 2015. His research interests include modal identification, wide-area monitoring system (WAMS) application, and operation and control of power systems.

Guillermo Bolivar-O. received the B.Eng. degree in electrical engineering from National University of Colombia, Medellin, Colombia, in 1985, and the master's degree in engineering from University of Manizales, Manizales, Colombia, in 2013. He is currently the Dean of Engineering Faculty at Corporación Universitaria Minuto de Dios, Bello, Colombia-UNIMINUTO. His current research interests include power distribution network and renewable energy.